NMR Structure Refinement and Dynamics of the K+−[d(G3T4G3)]2 Quadruplex via Particle Mesh Ewald Molecular Dynamics Simulations

ARTICLE *in* BIOPHYSICAL JOURNAL · SEPTEMBER 1998

Impact Factor: 3.97 · DOI: 10.1016/S0006-3495(98)77585-X · Source: PubMed

NMR Structure Refinement and Dynamics of the K^+-$[d(G_3T_4G_3)]_2$ Quadruplex via Particle Mesh Ewald Molecular Dynamics Simulations

Gary D. Strahan,* Max A. Keniry,# and Richard H. Shafer§

*Department of Pharmaceutical Sciences, University of Maryland, Baltimore, Maryland 21201; #Research School of Chemistry, The Australian National University, Canberra, Australia; and §Department of Pharmaceutical Chemistry, School of Pharmacy, University of California, San Francisco, San Francisco, California 94143-0446

ABSTRACT The solution structure and dynamical properties of the potassium-stabilized, hairpin dimer quadruplex formed by the oligonucleotide $d(G_3T_4G_3)$ have been elucidated by a combination of high-resolution NMR and molecular dynamics simulations. Refinement calculations were carried out both in vacuo, without internally coordinated K^+ cations, and in explicit water, with internally coordinated K^+ cations. In the latter case, the electrostatic interactions were calculated using the particle mesh Ewald (PME) method. The NMR restraints indicate that the K^+ quadruplex has a folding arrangement similar to that formed by the same oligonucleotide in the presence of sodium, but with significant local differences. Unlike the Na^+ quadruplex, the thymine loops found in K^+ exhibit considerable flexibility, and appear to interconvert between two preferred conformations. Furthermore, the NMR evidence points toward K^+-stabilized guanine quartets of slightly larger diameter relative to the Na^+-stabilized structure. The characteristics of the quartet stem are greatly affected by the modeling technique employed: caged cations alter the size and symmetry of the quartets, and explicit water molecules form hydration spines within the grooves. These results provide insight into those factors that determine the overall stability of hairpin dimer quadruplexes and the effects of different cations in modulating the relative stability of the dimeric hairpin and linear, four-stranded, quadruplex forms.

INTRODUCTION

The modeling of experimentally verifiable molecular structures often entails a number of hurdles. Quadruplexes in particular offer a uniquely difficult set of challenges, as many factors have been found to influence their structure. The type of stabilizing cation has long been associated with preferences for certain gross structural forms, determining whether a structure consists of four parallel strands, or one to two folded ones, in which some of the strands run antiparallel to others (Hardin et al., 1992; Williamson, 1994). The stabilization of specific structural forms, especially under biologically relevant concentrations of K^+ and Na^+, is of critical importance, as quadruplex complexes are being increasingly chosen as lead compounds for pharmaceutical development (Bock et al., 1992; Cherepanov et al., 1997; Mazumder et al., 1996).

Many studies have noted a correspondence between the size of the cation and the internal cavity between the quartet stacks, suggesting that cation coordination determines the stability and, perhaps, even the conformation (Guschlbauer et al., 1990; Hardin et al., 1991, 1992; Ross and Hardin, 1994; Sundquist and Klug, 1989). Others point to the hydration of the cation as the determining factor (Hud et al., 1996). In either case, the cation is a crucial component in the structure of these species, and the solvent is likely to be as well.

Typically, modeling of a DNA structure using NMR data does not involve the explicit treatment of solvent molecules, but relies instead on the experimental restraint set to embody all structure-influencing factors, and implicitly account for its presence. Similarly, the cations in such in vacuo simulations are usually considered only as neutralizing agents, but not as important influences on the structure; likewise, the hydration of the cation is not normally considered in determining the structure. Researchers working on accurate molecular refinement of quadruplex structures based upon NMR data should avoid making such assumptions.

The inclusion of cations in quadruplex molecular dynamics simulations is a unique challenge, because not only are the cations external to the molecule, but some are sandwiched within the stacked array of planar quartets and coordinate with the guanine bases. Although the exact location of the cations is unknown, there are some existing data concerning tightly bound cations. For example, in the crystal structure of the $[d(TGGGGT)]_4$ quadruplex, one sodium cation was associated with each interquartet region (Laughlan et al., 1994; Phillips et al., 1997). Similarly, a recent solution study on the linear quadruplex $[d(TGGGG)]_4$ reported at least three tightly bound potassium cations (Hardin et al., 1997). In agreement with this, $^{23}Na^+$ NMR studies (Deng and Braunlin, 1996) on the $d(G_4T_4G_4)$ hairpin dimer quadruplex revealed 2 ± 1 tightly bound Na^+ ions within this three-quartet system, and corroborated the conclusion that K^+ ions bind more strongly than Na^+ ions. The only x-ray study on a K^+-stabilized quadruplex (also the $d(G_4T_4G_4)$ hairpin dimer) revealed a single cation lo-

Received for publication 26 January 1998 and in final form 21 April 1998.

Address reprint requests to Dr. Richard H. Shafer, Department of Pharmaceutical Chemistry, School of Pharmacy, University of California, San Francisco, CA 94143-0446. Tel: 415-476-2761; Fax: 415-476-0688; E-mail: shafer@socrates.ucsf.edu.

0006-3495/98/08/968/14 $2.00

cated between the central pair of quartets (Kang et al., 1992). At this time, molecular modeling techniques do not provide a simple way to include the internal cations along with their occupancy probabilities. All prior NMR quadruplex structures were refined by ignoring these internal cations. Whereas our present in vacuo simulations do not include any coordinated cations, our solvated simulations include one full cation per quartet step, consistent with most of the solution data on tightly bound cations. In this way, a comparison may be made, providing insight into the effects of cation inclusion on both molecular stability and the ability of the resulting structures to satisfy NMR restraints.

When adjacent sites are thus occupied, the van der Waals surfaces of these cations are nearly touching each other, with neighboring cation centers at only ~3.5 Å separation (the same as the mean separation between the guanine quartets; Kang et al., 1992; Laughlan et al., 1994). It is difficult to model strongly charged ions in such close proximity unless long-range electrostatic effects are handled very carefully. Without such a treatment of Coulombic forces, trajectories will be unstable, resulting in distorted molecular geometries. One method of accurately modeling the long-range electrostatic effects, and hence providing stable trajectories that include both water and cations, is to use the particle mesh Ewald (PME) summation method (Essmann et al., 1995; Ewald, 1921), which has recently been included within the AMBER4.1 suite of programs (Pearlman et al., 1995).

As this is the first known instance in which solvated, PME-MD has been used simultaneously with NMR restraints to achieve a refined molecular structure, it is important to compare this methodology with the standard methods described above. This method of NMR refinement shows promise as a means of achieving highly realistic molecular structures and dynamical properties. The approach taken in this work was to first incorporate the NMR restraints into in vacuo molecular dynamics simulations without coordinated K^+ cations (non-PME)—as in the standard NMR refinement protocol—followed by continued refinement with simulations that include both explicit water and coordinated cations (using PME). This latter step has two parts. First, NMR restraints were imposed until the restraint energy appeared to converge (0.25–0.3 ns), followed by an unrestrained evolution period, during which the system was monitored to determine whether the NMR restraints were overconstraining the structure (0.45–0.5 ns). The ensembles of structures resulting from these independent trajectories were compared with the NMR data and to each other; the most probable set of structures, based upon the NMR data, was determined from each type of trajectory.

Because the goal of these simulations is the NMR refinement of the quadruplex structure using both solvent and coordinated cations, rather than a full characterization of the use of unrestrained PME-MD simulations, it was not necessary to perform very long trajectories. A time scale of ~0.75 ns (restrained and unrestrained) was chosen so as to balance the various requirements necessary for structure refinement, assessment of the stability of the trajectories, and adequate sampling of solvent density for investigation into effects of hydration. We note, however, that the unrestrained simulations were quite stable, and showed no trends that might suggest major structural changes at increased time scales.

From these simulations we derive important insights into the effects of water and cations on the NMR structure, as well as detail the causes of stability or flexibility within thymine loop structures, and their role in determining the overall stability of the molecular form. Quadruplex loops may be significant in other ways, as well, because they are involved in the association of the thrombin-binding aptamer with thrombin (Padmanabhan et al., 1993; Padmanabhan and Tulinsky, 1996), and their roles in other biochemical interactions have yet to be determined.

MATERIALS AND METHODS

Sample preparation

The decamer d(GGGTTTTGGG), a generous gift from Dr. Corey Levenson, was synthesized and prepared as described previously (Scaria et al., 1992). It was first purified by high-performance liquid chromatography using a triethyl ammonium acetate buffering system, and then dialyzed against 1 mM Tris (pH 7.5). This method of preparation avoids the use of either Na^+ or K^+, and results in samples free of metal cations. After dialysis, 4 ml of the sample was lyophilized and resuspended in 400 μl of 30 mM KCl, resulting in a 10 mM Tris (pH 7.5), 30 mM KCl solution. The sample was annealed after dilution with 4 ml of ^2H_2O, by heating to 90°C, followed by cooling to room temperature over 30 min. It was then lyophilized and redissolved in 400 μl of 99.996% ^2H_2O. For experiments with exchangeable protons, the same procedure was used, except that after lyophilization, the sample was redissolved in 90% H_2O/10% ^2H_2O.

Samples of the hairpin dimer quadruplex that were prepared in this manner were usable for ~48 h of 2D NMR experiments. After 48 h, NMR spectra showed evidence of a new, very different, slow-growing DNA species with significantly broader NOESY cross-peaks. As these new features were consistent with the greater correlation time of a much larger molecule, this new species was assumed to be a four-stranded, linear quadruplex. Circular dichroism spectra were consistent with a mixture of both types of quadruplexes. The linear quadruplex could be eliminated from the sample by another cycle of dilution, followed by annealing. This ensured that all 2D NMR studies discussed in this paper were performed only on samples consisting only of the hairpin dimer quadruplex, with no signs of the other kinetically unfavored species.

NMR spectroscopy

All NMR experiments were acquired at 500 MHz on a GE GN500 spectrometer, by the use of an Oxford Instruments magnet and a Nicolet 1280 computer. All 2D NMR experiments were performed at 20°C, except for NOESY experiments in 90% H_2O/10%^2H_2O, which were recorded at 2°C and 13°C, as well as 20°C. A spectral width of 10 kHz was used for the 90% H_2O/10%^2H_2O NOESY experiments, whereas 5208 Hz was used for the following ^2H_2O experiments: NOESY, double-quantum-filtered COSY (2QF-COSY), and homonuclear Hartmann-Hahn (HOHAHA) (Davis and Bax, 1985). A total of 4K complex data points were acquired for all 2D experiments, with 512 points in t_1 in all NOESY and HOHAHA spectra, and 800 points in t_1 for the 2QF-COSY spectra. In all experiments, 16 scans were accumulated for each point, with a 3-s delay.

All NOESY spectra were obtained in pure absorption mode with hypercomplex phase cycling and alternating block acquisition (States et al.,

1982), and time-proportional phase incrementation (Marion and Wuthrich, 1983) was used in the DQF-COSY and HOHAHA experiments. The NOESY spectra in ^2H_2O were acquired at three mixing times, 90, 150, and 220 ms, and a single mixing time of 150 ms was used for the 90% H_2O/10%^2H_2O NOESY spectra acquired at the three temperatures. Water suppression for the 90%H_2O/10%^2H_2O NOESY spectra was accomplished with an excitation pulse centered on $^1H^2HO$ and a short homospoil pulse during the mixing period (Hore, 1983); the excitation maximum was set between the imino and aromatic regions (at ~9 ppm). For the HOHAHA experiment, a 90-ms coherence transfer time was used. All data were processed on Sun workstations with locally written software. Data were apodized with either a Gaussian function with −7 Hz line-broadening and a shift of 20% for resolution enhancement, or a squared sine-bell function shifted by 45°, and were zero-filled to a final size of 4K × 2K.

Proton spin-lattice relaxation times T_1 were measured by the inversion-recovery method, employing a 180° composite pulse, with a repetition time of 30 s (Freeman et al., 1980). Spin-spin relaxation times, T_2, were determined by the Hahn spin-echo method.

Measurement of NOE cross-peak intensities

NOESY cross-peaks were assigned as described previously (Keniry et al., 1995; Strahan et al., 1994). Most peak volumes were determined by integrating the theoretical Gaussian fit to the peak of interest (Kneller, 1992). This method makes possible the deconvolution and integration of overlapping peaks. Volumes of the corresponding peaks on both sides of the diagonals were compared and averaged; if the intensity differed by more than twofold, then the more reliable value was determined by the goodness of the line fit. Low-intensity, nonoverlapping cross-peaks, having only a few data points, were integrated by an ellipsoid "boxing" method, which yields more reliable results in such cases. In this way, 500–630 cross-peaks were integrated within each of the NOESY spectra.

Quantitative NMR analysis

Interproton distances were estimated from integrated cross-peak intensities with the MARDIGRAS program (Borgias et al., 1990; Borgias and James, 1990). This program is based upon evaluation of the complete relaxation matrix. It incorporates all network relaxation and multispin effects, and provides reliable estimates of distances involving methyl protons (Liu et al., 1992). MARDIGRAS calculations were performed on integrated NOESY cross-peak data from all NOESY spectra (mixing times 90, 150, and 220 ms), using a range of correlation times between 2.0 and 3.5 ns. For each NOE peak, maximum and minimum restraint bounds were calculated, which were used for the molecular dynamics simulations. Because the spectral quality of the data obtained with a mixing time of 150 ms was superior to that obtained with the other two times, its integrated intensities were given greater weight in the final determination of restraint bounds. In all, 313 restraints were reliably derived from all of the NOESY spectra analyzed with MARDIGRAS.

As the orientation and placement of the strands could not be immediately discerned from a simple qualitative analysis of the NMR spectra, MARDIGRAS calculations were initially performed on a variety of different orientations. As described previously (Keniry et al., 1995; Strahan et al., 1994), these structural variants were generated by modifying the x-ray structure of $[d(G_4T_4G_4)]_2$, as obtained from the Brookhaven Protein Data Bank (file name 1D59) (Kang et al., 1992). These MARDIGRAS calculations converged to nearly identical interproton distances, indicating that the resulting set of 313 NOE-based restraints was essentially structure-independent.

As described previously (Keniry et al., 1995; Kim et al., 1992), the NOESY-based distance restraint set was augmented by secondary backbone restraints. These were used only to ensure physically reasonable structures during the in vacuo simulated annealing portion of the molecular modeling, and were removed during the in vacuo equilibration period to avoid overbiasing the structure with less reliable data. The secondary restraints were based on an analysis of the sum of the H4′ J-couplings ($\Sigma J_{H4'} = J_{H4'\text{-}H3'} + J_{H4'\text{-}H5'} + J_{H4'\text{-}H5''} + J_{H4'\text{-}P}$), H3′ J-couplings ($\Sigma J_{H3'} = J_{H3'\text{-}H2'} + J_{H3'\text{-}H2''} + J_{H3'\text{-}H4'}$) and linewidth analysis; where the experimental data were incomplete, comparisons with both the Na^+ form of the quadruplex and normal B-form DNA were used to provide approximations.

General molecular modeling methods

All energy minimization and molecular dynamics calculations were performed on a cluster of Hewlett-Packard HP-735 computers using the AMBER 4.1 suite of programs (Pearlman et al., 1995), with standard database files for partial charges and force field as previously reported (Cornell et al., 1995), except as noted below for the cations. Both the in vacuo and solvated simulations consisted of a brief simulated annealing protocol, followed by equilibration and evolution periods. NMR-derived restraints were used during both the in vacuo and first 0.25–0.3 ns of the solvated simulations, but were completely turned off for the remainder of the solvated simulations. The restrained molecular dynamics calculations made use of a pseudo-energy force field for the NOE-derived distance restraints having the form of a square well with parabolic sides. The width of the flat part of the well was derived from output of the MARDIGRAS program and was dependent on the agreement of the experimental and converged MARDIGRAS cross-peak intensity and on the signal-to-noise ratio (Liu et al., 1992). Secondary structure and backbone torsion angle restraints, determined from J-coupling data, were also used (with a similar pseudo-energy force field) for the simulated annealing portion of the in vacuo simulations; but they were not necessary during any portion of the solvated simulations and hence were not used (see below).

In vacuo restrained molecular dynamics

Preliminary quadruplex structures were neutralized by surrounding them with 18 pseudo-hexahydrated Na^+ counterions placed 5 Å from the backbone phosphate groups. Each of these counterions has a molecular weight equal to the sum of one Na^+ ion and six H_2O molecules (131 amu), an effective radius (r^*) of 5 Å (half the internuclear distance at the energy minimum), and a potential well depth (e) at r^* of 0.1 kcal-mol^{-1} (Pearlman et al., 1995). These in vacuo calculations did not include any internally coordinated cations. The electrostatic energy was evaluated using the distance-dependent dielectric function, $\epsilon = R_{ij}$, to mimic bulk solvent screening effects. Anomalous model building artifacts were removed from each of these structures by a combination of steepest descent and conjugate gradient energy minimization, followed by molecular dynamics simulations without restraints at a temperature of 10 K for 20 ps.

This was followed by restrained conjugate gradient energy minimization (rMIN) and in vacuo restrained molecular dynamics (rMD) simulations. These simulations were performed for 50 ps with a time step of 1 fs. All atoms within a 20-Å radius were included in nonbonded interactions, and during these initial simulations all bond lengths were constrained to their equilibrium values by the SHAKE algorithm (Ryckaert et al., 1977). Translational and rotational motions were removed every 50 fs. Initial velocities were assigned to a Maxwellian distribution at 10 K, with distance restraint force constants set to 1 kcal/mol-Å. The molecule was heated to 550 K, with NOE distance force constants concomitantly increased to 30 kcal/mol-Å over 10 ps. These conditions were maintained for 10 ps, after which the temperature and restraint force constants were reduced over 10 ps to 300 K and 20 kcal/mol-Å, respectively, then kept at these conditions for the remaining 20 ps.

During this annealing protocol, the secondary backbone torsional restraints were monotonically increased along with the temperature, from 0 kcal/mol-radian^2 to 50 kcal/mol-radian^2, then held steady during the high-temperature phase of the protocol, followed by a monotonic reduction back down to zero while the temperature was simultaneously lowered from 550 K to 300 K. The temperature was maintained by the Berendsen coupling algorithm (Berendsen et al., 1984) with separate solute-solvent and solvent-solvent coupling constants of 0.2 ps and 0.05 ps, where the pseudo-hexahydrated cations represent the external hydrated K^+.

In these in vacuo simulations (per standard NMR refinement procedure; Schmitz and James, 1995), the hydrogen bonds within the guanine quartets were reinforced by 24 distance restraints and 24 angle restraints, the force constants of which were always half the strength of the NOE distance restraints (see above). Coordinate sets were saved every 0.2 ps for each MD run, and the final 5 ps was averaged and energy minimized. Independent trajectories were achieved with the use of different initial random seeds for setting the Maxwellian distribution of velocities (Brahms et al., 1992).

Molecular dynamics simulations in water

Three in vacuo quadruplex structures satisfied the NMR restraints nearly equally well, and their coordinate sets were used for further refinement via solvated molecular dynamics simulations. For these solvated, PME MD simulations, the 18 pseudo-hexahydrated Na^+ cations that were employed in the in vacuo rMD simulations were replaced by 18 explicit K^+ cations; 16 of these K^+ were placed in the solution near the phosphates of the DNA backbone, while the remaining two were sandwiched between the quartets of the in vacuo quadruplex structures at the approximate positions of those (central-quartet) coordinated cations, which have been observed in x-ray structures (Kang et al., 1992). The values of r^* and e were chosen (1.93 Å and 0.1 kcal-mol^{-1}, respectively) in accordance with the parameterization of K^+ by Ross and Hardin (1994).

Each of the three K^+-DNA, solute-plus-counterions systems was immersed in water boxes 9 Å larger than the quadruplex molecule, with a final size of 50 Å × 45 Å × 45 Å and consisting of 2766 TIP3P water molecules. The system was minimized with positional and NMR NOESY restraints to hold the DNA in place during a series of energy minimizations and restrained dynamics simulations (Cheatham et al., 1995). The force constant strength of the positional restraints was serially decreased to facilitate the systematic equilibration of the water-DNA system, and the NMR NOESY restraints helped maintain its fit to the experimental data. Whereas the in vacuo simulations required artificial reinforcement of the quartet hydrogen-bonding to maintain the integrity of the structure throughout the simulations by avoiding spurious high velocities (e.g., localized hot spots), the solvated PME-MD simulations were extremely stable without these artificial restraints, and hence they were not used. Similarly, the use of explicit solvent negated the need for repulsive restraints, as well as secondary structure, backbone torsion angle restraints (see discussion above).

Each structure was then reannealed by a protocol similar to that described in the in vacuo section, to allow the model to simultaneously adjust to both the NMR NOESY restraints and the presence of water and K^+ ions. The system was heated to 500 K and kept there for 5 ps, while the NMR restraint force constants were held at 30 kcal/mol-Å^2 and then cooled to 300 K, while the force constants were reduced to 10 kcal/mol-Å^2. After equilibrating at 300 K, the system was maintained at that temperature for an additional 0.25–0.3 ns, until the restraint energy appeared to be equilibrated. Then the NMR NOESY restraints were monotonically decreased over 20 ps to a final force constant strength of 0 kcal/mol-Å^2. To determine whether the ensemble of NMR restraints overconstrained the structure, and to provide sufficient sampling of the solvent for hydration analysis, the simulations were continued for 0.45–0.5 ns without restraints. SHAKE (Ryckaert et al., 1977) was applied to all bonds involving hydrogen atoms. The pressure of the system was 1 atm, and the temperature was maintained by the Berendsen coupling algorithm (Berendsen et al., 1984), with separate solute-solvent and solvent-solvent coupling constants of 0.2 ps for each. An integration time step of 2 fs was used, and the nonbonded pair list was updated every 10 steps.

These explicit solvent rMD simulations were performed by the particle mesh Ewald (PME) summation method developed by Essmann et al. (1995) for calculating Coulombic interactions; this evaluates the full electrostatic energies within a unit cell in a macroscopic lattice of infinitely repeating images. The PME grid spacing was ~1.0 Å; it was interpolated on a cubic B-spline with the direct sum tolerance set to 10^{-5}. The Lennard-Jones interactions were subjected to a 9-Å cutoff.

The current implementation of PME within AMBER4.1 neglects the imaging of atoms in NMR restraints, causing severe, artificial molecular distortion when a portion of the molecule wanders out of the periodic box and wraps to the other side. To alleviate this, the molecule was centered in the box, and a weak, 2-kcal/mol-Å^2 positional restraint was arbitrarily placed on one C4 atom in the central quartet. This not only circumvented the imaging artifact, but also negated the growth of center-of-mass velocities, which occurs as an artifact of the Berendsen coupling algorithm and incomplete energy conservation (Harvey et al., 1998). This method was used even during the unrestrained simulations to maintain consistency. No structural aberrations resulted from this additional restraint.

The trajectories were analyzed using a variety of in-house scripts and CARNAL, a module of AMBER 4.1. Time-averaged structures were calculated with CARNAL, followed by a 100-step minimization, to restore the fast moving methyl protons to a realistic geometry without altering any other structural details, as indicated by a "before-and-after" all-atom RMS of nearly zero Å.

The ensemble of structures over the time course of the simulations was compared to experimental NMR intensities by using ensemble CORMA 5.01 and PARSE (Ulyanov et al., 1995) to select those coordinate sets from each MD simulation that together best satisfy the NMR restraints. In this way, coordinate sets from several trajectories can be combined to determine whether the NMR restraints are biased toward one type of conformation, or include a percentage of each.

The calculation of solvent and counterion distributions closely followed recently published methods (Cheatham and Kollman, 1997) in which the positions of interesting atoms (e.g., water oxygen atoms) are binned into (0.5 Å)^3 grids from 1-ps-interval trajectory frames, in which the DNA atoms have been RMS coordinate fit to the initial structure. This "binning" was performed over the entire ~0.75 ns of the solvated PME MD simulations, including both the NMR restrained and unrestrained segments. Each grid element, therefore, is a summation over time, representing the frequency with which the center of a particular atom type (e.g., water oxygen) occurs within the grid element. These grids were contoured using the density delegate of UCSF MidasPlus (Ferrin et al., 1988). Assuming bulk water density, the calculated number of water molecules expected per grid element, for 750 frames, is 3.14. In the graphics of water oxygen atoms, the contouring of the water oxygen density was performed at 9.0 hits/0.5 Å^3, or approximately three times the expected bulk water density.

RESULTS AND DISCUSSION

Previous studies on the quadruplexes formed by $[d(G_3T_4G_3)]_2$ in Na^+ versus K^+ have noted important differences in their chemical shifts and NMR NOESY contacts (Keniry et al., 1995; Smith et al., 1994; Strahan et al., 1994). Table 1 lists the nucleotide proton chemical shifts determined for the nonexchangeable protons in the K^+-$[d(G_3T_4G_3)]_2$ quadruplex. Only the nonexchangeable data were quantified and incorporated into the various molecular dynamics simulations to produce refined structures. However, the qualitative aspects of the exchangeable data were critical in the final analysis of the correct geometry.

Initially, many different quadruplex structures were generated, each with different folding patterns, but consistent with preliminary experimental evidence (Scaria et al., 1992). To determine which folding pattern best fit the NMR data, restrained molecular dynamics simulations were performed, and those models that could not reasonably satisfy the NOESY distance requirements were excluded from additional consideration. NMR distance restraints were applied to the various model structures via in vacuo energy minimization and 50 ps of molecular dynamics simulations

TABLE 1 Nucleotide proton chemical shifts of the K^+-$[d(G_3T_4G_3)]_2$ quadruplex (in ppm)

Strand	Nucleotide	H8/H6	H5	H1′	H2′	H2″	H3′	H4′	H5′/H5″	H1/H3	Amino[b]
1	G1*syn*	7.29	—	6.08	3.13	3.31	5.00	4.50	4.18, NA	11.68	10.32, 6.55
	G2*syn*	7.50	—	5.78	2.42	2.45	5.06	4.20	4.30, NA	NA	NA
	G3*anti*	7.95	—	6.07	2.55	2.68	4.99	4.50	4.18, NA	11.63	NA
	T4	7.08	1.81	5.68	1.53	2.18	4.62	3.99	4.10, 4.38	NA	—
	T5	7.31	1.62	5.57	1.99	2.00	4.57	3.59	3.66, 3.58	NA	—
	T6	7.22	1.50	5.53	1.80	2.28	4.55	4.41	3.91, 4.04	NA	—
	T7	7.51	1.77	6.12	2.06	2.44	4.67	3.18	3.06, 2.84	NA	—
	G8*syn*	7.61	—	6.18	3.65	3.06	4.97	4.55	4.21, NA	NA	9.56, 6.54
	G9*anti*	8.04	—	5.99	2.59	2.78	5.11	4.47	4.38, NA	NA	NA
	G10*anti*	7.93	—	6.43	2.60	2.53	4.73	4.39	4.11, NA	NA	NA
2	G11*syn*	7.43	—	5.93	2.84	3.08	5.00	4.48	4.11, 3.96	11.81	10.39, 6.47
	G12*anti*	8.08	—	5.69	2.54	2.58	5.11	4.34	4.23, NA	NA	NA
	G13*anti*	7.83	—	6.19	2.55	2.75	5.01	4.55	4.22, 4.22	11.62	NA
	T14	7.19	1.83	5.71	1.75	2.23	4.66	4.02	4.12, NA	NA	—
	T15	7.35	1.66	5.69	1.91	1.92	4.55	3.67	3.68, NA	NA	—
	T16	7.25	1.47	5.70	1.91	2.19	4.51	3.89	3.90, 3.79	NA	—
	T17	7.40	1.75	5.96	1.98	2.40	4.56	3.43	3.19, 2.73	NA	—
	G18*syn*	7.49	—	6.20	3.84	3.28	4.94	4.42	4.18, 4.37	NA	NA
	G19*syn*	7.53	—	5.94	2.81	2.64	5.12	4.30	4.39, NA	NA	NA
	G20*anti*	8.17	—	6.27	2.59	2.29	4.75	4.31	4.43, NA	NA	NA

NA, Not assigned. Amino and imino resonance assignments were determined by comparison with refined model structures.
*Contacts between nonexchangeable loop protons and five additional imino protons, as well as several amino protons, were observed but could not be definitively assigned.

using the annealing protocol described and the AMBER 4.1 suite of programs. High-restraint violations allowed for the exclusion of several models, but the qualitative information obtained from the exchangeable ^{1}H NMR data singled out one of the models as being the only one capable of explaining all of the information, as described previously for the Na^+-stabilized quadruplex (Keniry et al., 1995).

Four independent, in vacuo, restrained molecular dynamics simulations were performed, starting with the best-fitting model and using different sets of random initial velocities. These improved in vacuo simulations resulted in a family of closely related structures; their general folding topology is depicted in Fig. 1. These structures varied the most in the conformations of their thymine loops, which stretch across the diagonal of the outermost guanine quartets. The general arrangement of the strands and positions of the deoxyguanosine glycosidic bond angles were the same as those found in the Na^+-stabilized structure described elsewhere (Keniry et al., 1995; Smith et al., 1994; Strahan et al., 1994). The sequential arrangement of the *syn* (S) and *anti* (A) deoxyguanosines is

strand 1: $G1_S$-$G2_S$-$G3_A$-T4-T5-T6-T7-$G8_S$-$G9_A$-$G10_A$

strand 2: $G11_S$-$G12_A$-$G13_A$-T14-T15-T16-T17-$G18_S$-$G19_S$-$G20_A$.

It is interesting that these two strands are identical in nucleotide sequence, yet, when brought together, prefer a molecular topology that is asymmetrical, as observed in the sequential arrangement of guanosine glycosidic bond angles. In principle, an exchange should occur between these two strands, but no evidence for this has been observed.

The guanine quartet stem regions of the structures resulting from the four in vacuo rMD simulations appeared qualitatively similar, and had an average, pairwise, heavy-atom root mean square deviation (RMSD) (not mass-weighted) of 0.78 Å. The thymine loops exhibited visually significant differences within their stacking arrangements; their inclu-

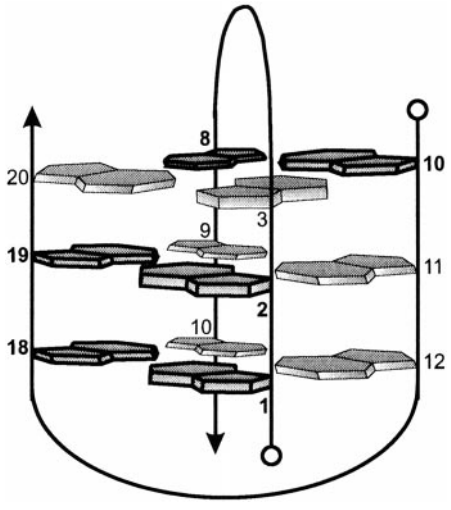

FIGURE 1 Schematic drawing of the $[d(G_3T_4G_3)]_2$ dimeric hairpin quadruplex. Within any given quartet, the deoxyguanosines have *syn* (S) and *anti* (A) glycosidic bond angles, which vary as S-S-A-A. As described in the text, the sequential arrangement of dG glycosidic bond angles is not symmetrical, resulting in two types of quartet steps: those in which the base steps are either 5′-*syn*-*syn*-3′ or 5′-*anti*-*anti*-3′, forming the S-S/A-A quartet stack, and those in which all base steps are 5′-*syn*-*anti*-3′, forming the S-A quartet stack. Dark (light) bases denote *syn* (*anti*) deoxyguanosines.

sion in the calculation increased the pairwise RMSD to 1.18 Å. Each of the two loops per complex is able to adopt two different types of conformations, satisfying two different subsets of NMR restraints. Only a few restraints appeared to be unique to each subset, whereas the other restraints worked together with the subsets in a concerted manner (see below). These two conformations are hereafter referred to as "quartet stacked" when either thymine 7 or 17 is directly stacked over some portion of an outermost quartet, and "unstacked" when thymine 7 or 17 is pointing outward into solution, with its methyl group roughly stacked over thymine 5 or 15 (see Fig. 2). The two thymine loops were capable of adopting similar conformations, suggesting that most of the molecular asymmetry is localized in the quartet stem.

To clarify the influence of cations and solvent on both the quartet stem and loops, the simulations were continued by using both explicit H_2O molecules and internally coordinated, or "caged," K^+ cations. Three of the refined in vacuo structures were chosen for these studies. One structure had both loops in a "quartet stacked" conformation, the second structure had one loop "quartet stacked" and the other one "unstacked," and the third structure had both loops "unstacked." These three structures defined three trajectories, A, B, and C, respectively. Two explicit K^+ cations were positioned by visual inspection between the three quartets, in the approximate position previously determined by x-ray studies (Kang et al., 1992). The models were then immersed in water boxes (as described in Materials and Methods) and energy minimized with NMR restraints and PME. This was followed by an annealing protocol (30 ps), 20 ps of equilibration, and 0.25–0.3 ns of restrained MD with PME (these trajectories are henceforth termed rA, rB, and rC). This was continued as unrestrained, solvated, PME-MD simulations for an additional 0.45–0.5 ns (termed uA, uB, and uC). It should be noted that MD simulations on these solvated molecules without PME, using the standard AMBER 4.1 electrostatic cutoffs (Pearlman et al., 1995), resulted in unstable trajectories, wherein extreme molecular distortion occurred before 100 ps.

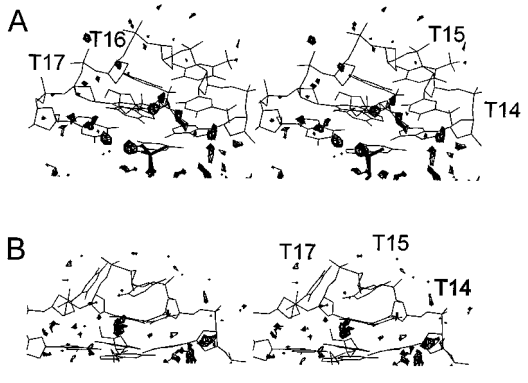

FIGURE 2 Stereo images of the two possible loop conformations, with contoured regions of calculated water density higher than average (3×). The loop in *A* depicts T17 "quartet stacked" over the outermost quartet, whereas T15 forms the top of a triangle consisting of T14, T15, and T17. The calculated water density is localized just outside of the front of this triangle. The loop in *B* depicts T17 "unstacked," partially protruding into the solvent, and with its methyl group resting over T15. The hydrogen bonding acceptor and donor groups of T15 are pointing downward toward the region of high water density, which, in turn, is stabilized by interactions with the K^+ ion in the cavity of the quadruplex stem. T16 is behind T17 in *B*, which obscures it from view, and hence it is not labeled.

The ensembles of structures generated by each of the simulations were analyzed independently and as groups, and divided according to whether or not they were performed in vacuo or solvated with PME-MD, and whether or not they utilized NMR restraints. Thus the solvated PME-MD simulations were analyzed as two "cross-simulation ensembles." Group 1 consisted of rA, rB, and rC, and Group 2 consisted of uA, uB, and uC. In addition to RMSD comparisons of the time-averaged structures from each trajectory, the PARSE algorithm (Ulyanov et al., 1995) was used to identify the fewest number of structures within each cross-simulation group that best fit the NMR NOESY data; it calculated the relative probabilities of the identified structures and produced a "best-fit" ensemble. How well each trajectory and "PARSE" ensemble satisfies the NMR NOESY data was evaluated by calculating the standard and sixth-root *R* factors with CORMA 5.01. The low *R*-factor values found in Table 2 indicate that all of the groups of structures are generally in good agreement with the NMR data, but in vacuo and solvated structures differ in important details, especially the hydrogen bonding and hydrophobic regions in the loops, and hydration spines along the quartet stem (see below).

Although the restrained in vacuo structures fit the NMR data reasonably well (Table 2), their *R* factors reflect the fact that static models cannot adequately account for the observed conformational variations and flexibility, nor are the NMR restraints alone sufficient to properly adjust the structure for the presence of water molecules and coordinated cations. The reliability of these in vacuo structures is also compromised by structural anomalies in the quadruplex stem and thymine loops. The inclusion of explicit water and caged K^+ cations in the PME-MD simulations removes these anomalies (see below), and conformational sampling over longer solvated, restrained PME-MD trajectories can produce ensembles of structures with *R*-factors smaller than those of the in vacuo simulations. The "PARSE" cross-simulation, solvated PME-MD ensembles have improved interresidue *R*-factors because they consist of a series of selected structures (along with their probabilities) that cover an optimal range of conformations that best fit the NMR data, and thus better approximate the real solution ensemble. Hence the real structures in solution, as measured by NMR, are likely to be a mixture of the conformations sampled by these ensembles.

Coordinate averaging over each trajectory produced time-averaged structures for both the restrained (rMD) and unrestrained (uMD) sets of simulations. These structures can be compared to each other by calculating their pairwise RMSD. The time-averaged structures from the restrained

TABLE 2 The standard *R* factors and sixth-root residual indices (R_1^x) comparing the ensembles of structures from the in vacuo and solvated, PME-MD simulations to the NOESY cross-peak intensities at three different mixing times

Mixing time (ms)	$R_{\text{intra-res.}}$	$R_{\text{inter-res.}}$	R_{total}	$R^x_{1\,\text{intra-res.}}$	$R^x_{1\,\text{inter-res.}}$	$R^x_{1\,\text{total}}$	Trajectory*
The average *R* factors of the four, time-averaged structures resulting from the four restrained in vacuo MD simulations (A–D)							
220	0.340	0.770	0.382	0.063	0.121	0.081	A–D in vacuo
150	0.290	0.671	0.333	0.058	0.115	0.074	A–D in vacuo
90	0.432	0.844	0.458	0.073	0.298	0.102	A–D in vacuo
Ensemble *R* factors for the restrained PME-MD simulations with explicit H_2O and caged K^+. The PARSE ensemble consists of structures from each of the three trajectories in the following proportions: 9% rA1, 15% rA2, 13% rB, and 62% rC							
220	0.343	0.633	0.375	0.066	0.109	0.077	rA1 PME-MD
	0.350	0.620	0.380	0.067	0.109	0.078	rA2
	0.348	0.575	0.372	0.067	0.102	0.076	rB
	0.345	0.581	0.371	0.067	0.101	0.075	rC
	0.332	0.533	0.354	0.064	0.098	0.073	PARSE ensemble
150	0.266	0.455	0.289	0.055	0.096	0.067	rA1
	0.266	0.408	0.283	0.055	0.091	0.065	rA2
	0.260	0.386	0.275	0.057	0.089	0.066	rB
	0.265	0.435	0.286	0.058	0.092	0.068	rC
	0.256	0.374	0.271	0.053	0.087	0.064	PARSE ensemble
90	0.451	0.600	0.457	0.079	0.289	0.101	rA1
	0.466	0.592	0.470	0.081	0.291	0.102	rA2
	0.454	0.626	0.460	0.078	0.295	0.101	rB
	0.464	0.636	0.471	0.077	0.299	0.102	rC
	0.453	0.509	0.455	0.077	0.285	0.098	PARSE ensemble
Ensemble *R* factors for the unrestrained continuations of the PME-MD simulations using explicit H_2O and caged K^+. The PARSE ensemble consists of structures from each of the three trajectories in the following proportions: 30% uA2, 19% uB, and 51% uC							
220	0.334	0.877	0.393	0.067	0.168	0.093	uA2 PME-MD
	0.328	0.926	0.393	0.063	0.158	0.087	uB
	0.312	0.817	0.367	0.058	0.144	0.080	uC
	0.316	0.799	0.364	0.060	0.143	0.081	PARSE ensemble
150	0.297	0.700	0.347	0.066	0.171	0.096	uA2
	0.281	0.721	0.335	0.066	0.171	0.095	uB
	0.268	0.632	0.313	0.063	0.144	0.086	uC
	0.259	0.602	0.301	0.060	0.147	0.084	PARSE ensemble
90	0.466	0.568	0.470	0.086	0.285	0.106	uA2
	0.457	0.800	0.470	0.082	0.308	0.105	uB
	0.441	0.613	0.448	0.076	0.290	0.099	uC
	0.446	0.511	0.448	0.079	0.280	0.100	PARSE ensemble

The molecular modeling refinement process more heavily weighted the superior integrated intensities of the 150-ms spectrum (see text).
*The restrained segment of trajectory A was analyzed in two segments (rA1 and rA2) because of an important conformational change that occurred during the simulations (see text). As a result of the conformational change, trajectory segments rA2 and rB are structurally very similar, as are uA2 and uB.

simulations (rA, rB, and rC) differ from each other by an average pairwise RMSD of 0.98 Å (SD = 0.13), when all heavy atoms are considered (not mass weighted), whereas the time-averaged structures from the three unrestrained simulations (uA, uB, and uC) differ from each other by an average of 1.16 Å (SD = 0.18). The pairwise RMSD is reduced almost by half when only the stem guanines are considered, consistent with the structural variability of the thymine loops: the pairwise RMSD (stem only) between the time-averaged structures for both the rMD and uMD simulations is 0.66 Å (SD = 0.15 and 0.16, respectively). (For these analyses, simulation rA had to be considered as two parts, rA1 and rA2, because the conformation of the T4–T7 loop changed after ~100 ps from quartet stacked to unstacked. Simulation rA2 was continued as the unrestrained simulation uA2 or, simply, uA.)

Releasing the NMR restraints from the trajectories produced time-averaged structures that drifted an average of 1.37 Å (SD = 0.12) away from the corresponding time-averaged, restrained structures. Two-thirds of this drift was due to subtle changes in the quadruplex stem, which drifted an average of 1.01 Å (SD = 0.16) as it relaxed. The remaining third of this drift resulted from changes within the loops as they interacted with the solvent and coordinated K^+ ion. Most of this drift occurred during the first 100 ps after removal of the restraints, after which the trajectories remained very stable. This drift consists of a complex set of slight movements of the model structure away from a representation of the ensemble-averaged, NMR structure in solution, and toward that of a single structure.

All of the solvated, PME-MD simulations, even unrestrained, remained remarkably close to the distances calculated from the NMR data. The average deviation of the interproton distances within the rMD trajectories from the calculated closest distance boundary, as determined by MARDIGRAS and based upon the NMR data, was 0.10–

0.15 Å. The gradual complete removal of the NMR restraints (over 20 ps) perturbed the system, producing a transitional period of less than 100 ps, during which the average of the distance deviations from the closest NMR boundary was 0.22–0.30 Å. After this transitional period, however, all three trajectories settled down to an averaged distance deviation of 0.17–0.25 Å.

The quadruplex stem

Whereas the exchangeable proton NOESY spectra of the Na^+-$[d(G_3T_4G_3)]_2$ quadruplex (Keniry et al., 1995) had many assignable cross-peaks, the corresponding spectra of the K^+ form had fewer (even at 2°C), and those that were observed were very broad. Similarly, the K^+ stabilized quadruplex had fewer interresidue G(H8)-G(H8) NOESY contacts compared to the Na^+ stabilized structure (data not shown). These spectral differences can be attributed to the size of the coordinating cation and the extent to which the quadruplex guanines can contract around it, affecting the orientation and strength of the hydrogen bonds (Ross and Hardin, 1994).

In the quadruplex structure, the size of the internal cavity is a crucial parameter that influences the helical parameters, groove widths, and backbone angles; it is within this cavity that the cation resides. The size of this cavity is best evaluated by the interquartet distance (or quartet rise, which is calculated as the distance between the geometric centers of the adjacent planes; Schultze et al., 1994) and the O6-O6 distances for guanine bases located diagonally across from each other in the same quartet. These parameters vary significantly, depending on the use of restraints and the inclusion of internally coordinated K^+ ions.

The average interquartet rise for the S-S/A-A quartet step (see Fig. 1) is 3.37 Å in the restrained in vacuo simulations that lack internally coordinated K^+ ions. The use of "caged" K^+ ions increases this distance by ~0.2 Å to 3.55 Å for both restrained and unrestrained solvated, PME-MD simulations. However, the average S-A quartet step (Fig. 1) distance remains essentially unchanged by the use of caged K^+ ions, changing from 3.36 Å to 3.39 Å. The inclusion of caged K^+ causes the inner diameter of all of the quartets (as measured by the intraquartet, diagonal O6-O6 distance) to decrease by an average of nearly 1 Å.

This decrease in the inner quartet diameter is less significant, perhaps, than the change that occurs in the shape of the quartet. All structures generated by in vacuo simulations with NMR restraints and lacking internally coordinated cations (both those described in this work, as well as in our earlier work on the Na^+-stabilized form; Keniry et al., 1995) contain asymmetrical quartets in which the average diagonal intraquartet O6-O6 distance is ~5.7 Å in one direction, but ~4.7 Å in the perpendicular direction. The inclusion of the caged K^+ helps reduce this asymmetry. The restrained, solvated simulations (rA1, rA2, rB, and rC) with caged K^+ exhibit nearly symmetrical external quartets (~4.6 Å in both dimensions), but the central quartet remains asymmetrical (~3.8 Å and ~5.8 Å); in contrast, the unrestrained, solvated simulations with caged K^+ (uA2, uB, and uC) produce three almost perfectly symmetrical quartets (~4.3 Å in both directions) similar to those found in the x-ray structure of $[d(TGGGGT)]_4$ (Laughlan et al., 1994).

The average "twist" of the quartets (calculated as the angle between the vectors from the C1′ coordinate and the geometric center, in two adjacent planes; Laughlan et al., 1994) appears to be correlated with the interquartet distance, or quartet rise. The S-S/A-A quartet step changes more significantly with the modeling protocol than does the S-A quartet step. The in vacuo simulations produce structures that have a S-S/A-A quartet step with an average twist angle of 26° (SD 3°); the restrained, solvated simulations with caged K^+ (rA1, rA2, rB, and rC) have an average S-S/A-A quartet step twist angle of 22° (SD 5°), and the unrestrained, solvated simulations with caged K^+ (uA2, uB, and uC) have an average S-S/A-A twist angle of 25° (SD 3°). By comparison, the S-A quartet step in the in vacuo simulations has an average twist angle of 20° (SD 3°) and barely increases to 23° (SD 3°) for both the rMD and uMD simulations in solution with caged K^+. Solvation effects may be important influences on these twist values, as there is a region of higher than normal water concentration at this S-A quartet step, which is not present at the S-S/A-A quartet step (see below). Considering the manner in which the twist parameter is calculated, its value is also influenced by the relative positions of the C1′ atoms and hence may be affected by the increased quartet symmetry when caged K^+ ions are used in the solvated PME-MD simulations.

As with previous solution studies of dimeric hairpin quadruplexes, all of the simulations described here indicate that the quadruplex formed in the presence of K^+ has three different groove widths. These grooves also demonstrate variability depending on the conditions of the simulations, as shown in Table 3, although no clear pattern is discernible.

Solvation of the DNA phosphate groups and guanine amino groups, as well as the attraction of water to the caged K^+ ions, can combine to produce well-defined water spines in the grooves, which in turn are important influences on groove widths, backbone angles, and hence the helicoidal structure. Fig. 3 shows stereo views of the average structures from the last 0.3 ns of trajectories uA2, uB, and uC. Also displayed in this figure are regions of greater than average water density. The water box was divided into (0.5 Å)^3 grid boxes, and each occurrence of a water oxygen atom within a grid box was summed over the entire time course (~0.75 ns) of restrained and unrestrained simulations in solvent (Cheatham and Kollman, 1997). The resulting grids can be considered as water probability maps depicting local regions of greater than normal water concentration. In this figure, these water density maps are contoured to reveal those regions where water molecules reside about three times more frequently than expected at normal, bulk water concentration. The presence of these areas of high water

TABLE 3 Groove widths of the average quadruplex structures

	Modeling properties			Average groove widths in Å (S.D.)			
Trajectories averaged*	Explicit H_2O	NMR restraints	Caged cation	Wide	Medium 1	Medium 2	Small
Na^+: in vacuo[#]	No	Yes	No	13.1	8.2	7.3	5.3
K^+: in vacuo	No	Yes	No	13.4 (.2)	6.0 (.8)	7.9 (.4)	5.8 (1)
rA, rB, rC	Yes	Yes	Yes (K^+)	12.4 (.5)	6.6 (.6)	9.9 (.3)	6.3 (1.5)
uA, uB, uC	Yes	No	Yes (K^+)	13.0 (.2)	6.1 (.4)	7.1 (.04)	4.2 (1.1)

All distances are between phosphorus atoms separated by one quartet step, regardless of whether a closer phosphorus atom exists (see Discussion). Values in parentheses are standard deviations.

*To improve statistics, the distances from the time-averaged structures within each trajectory were averaged with those from the same modeling category.

[#]Measured from the model by Keniry et al. (1995). Because only one model was measured, no standard deviation statistics could be determined.

probability suggests that water spines form within most of the grooves.

One region of calculated high water concentration occurs in medium groove 1 at G2, where the phosphate and sugar oxygen atoms form a "cage" around water density that has accumulated near the G2 and G20 amino groups in the S-A quartet step (Fig. 4). The water appears to be attracted to this region of the molecule, because these amino groups lie next to each other, providing more opportunities for hydrogen bonding than can be found in other steps, such as in the

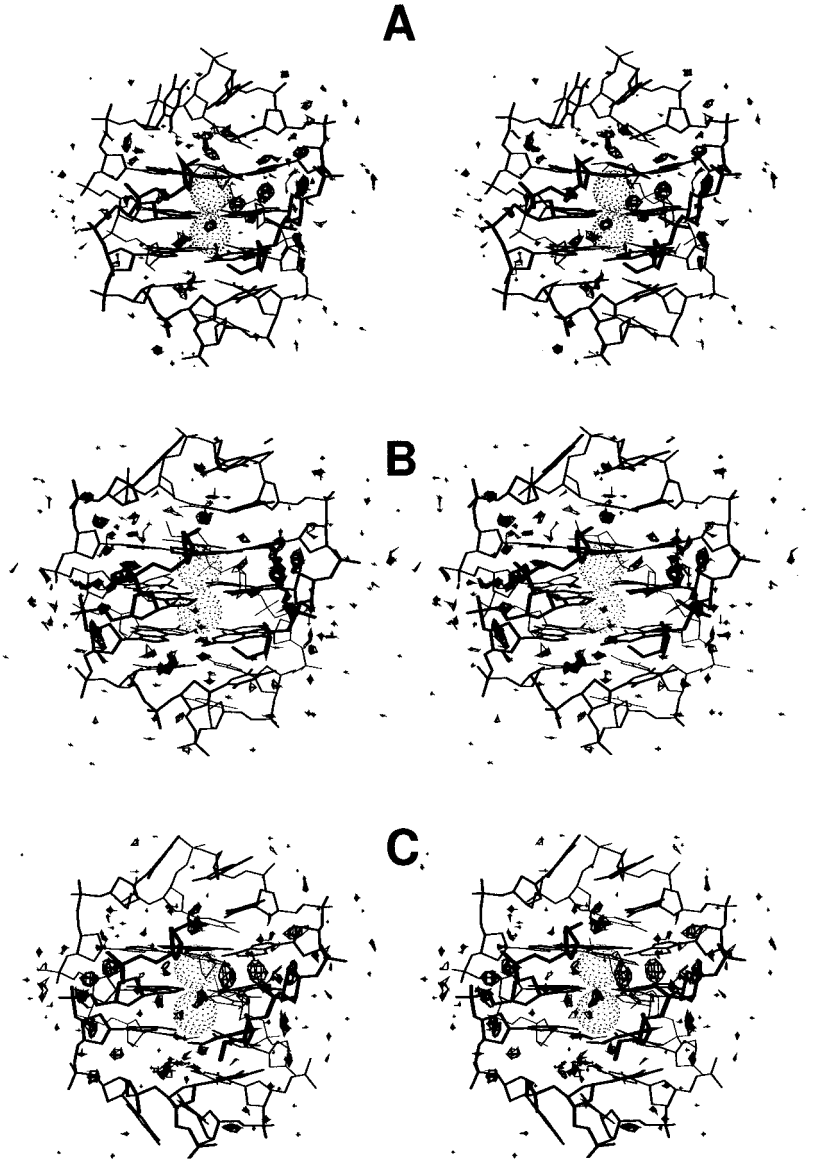

FIGURE 3 Stereo views of the average structures from the last 0.3 ns of trajectories uA2, uB, and uC (*A*, *B*, and *C*, respectively), along with contoured regions of calculated greater than average (3×) water density. Besides those loop regions with greater than average water density, close inspection reveals several regions within the grooves of the quadruplex stem.

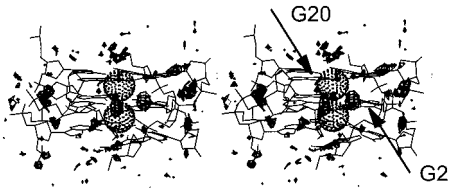

FIGURE 4 Medium groove 1 between G2 and G20, where the phosphate and sugar oxygen atoms form a kind of cage around higher than average (3×) water density which has accumulated around the amino groups in the S-A quartet step. The phosphate group partially shields these waters from the bulk of the solvent.

S-S/A-A quartet step, which does not stabilize a water density pocket. An inwardly bent phosphate group partially shields these waters from the bulk of the solvent, producing the most stable of all of the water-binding sites in these simulations—it is present in all simulations and most of the time steps. This inwardly bent phosphate group is suggested by the restrained in vacuo simulations, but becomes more clearly defined in the presence of water. Interestingly, neither of these last two features can be correlated with unusual backbone torsions—the backbone torsions for all simulations are generally very comparable to those previously published (Keniry et al., 1995; backbone torsions are available from the authors upon request).

Another region of higher than normal calculated water concentration is associated with an unusually short phosphorus-phosphorus distance between G9 and G19 in the smallest groove—a distance of 2–3 Å, depending on the model, after subtraction of 5.8 Å for the combined radii of the phosphorus atoms. This structural feature is observed in all $[d(G_3T_4G_3)]_2$ quadruplex structures determined to date, regardless of whether the simulations were performed in vacuo or in solvent, or whether restraints were used, or whether those restraints were measured from solutions containing K^+ or Na^+ (Keniry et al., 1995). The present simulations in water offer an explanation for this short distance, as the O5′ of G19 appears to be interacting with water molecules that are stabilized between it and the amino group of the same guanine, thus bending the phosphate group toward the middle of the groove. The crystal structure of $[d(G_4T_4G_4)]_2$ (Kang et al., 1992) also had phosphate groups that were rotated inward to form hydrogen bonds with guanine amino protons, but the crystal structure gave no evidence of the presence of mediating water molecules.

Loop conformation and flexibility

The K^+ quadruplex stacks T5 over T4, which is, in turn, stacked over G3. This general stacking pattern is similar to that found in the Na^+ form of the $[d(G_3T_4G_3)_2]$ quadruplex (Keniry et al., 1995) and the stacking interactions of hairpin loops with duplex DNA stems (Haasnoot et al., 1986, 1987). However, in the unstacked K^+ loop conformation, the T5 base is not parallel to the quartets, but is instead tilted downward to establish water-mediated hydrogen bonding interactions with the cation.

In all of the loop conformations for the K^+ quadruplex, the NMR NOESY data indicate that T6 is stacked over the first guanine of the other strand (the nonsequential G11, as shown in Fig. 5). Its methyl group points inward to establish a hydrophobic pocket with T4 and T5, and its hydrogen bonding groups point outward into the solution—this is the exact opposite of what was determined from the NMR data of the Na^+-stabilized structure (Keniry et al., 1995). These differences may result from a comparatively shallower loop in K^+, as it stretches across a wider diagonal (see below).

Our initial interest in the loops of this structure arose from the observation that several intraresidue NOESY cross-peaks relating to T7 and T17 are broader than any other similar cross-peaks. Examples include the broad H6-methyl NOE contacts (Fig. 5) and the weak H6-H1′ contacts

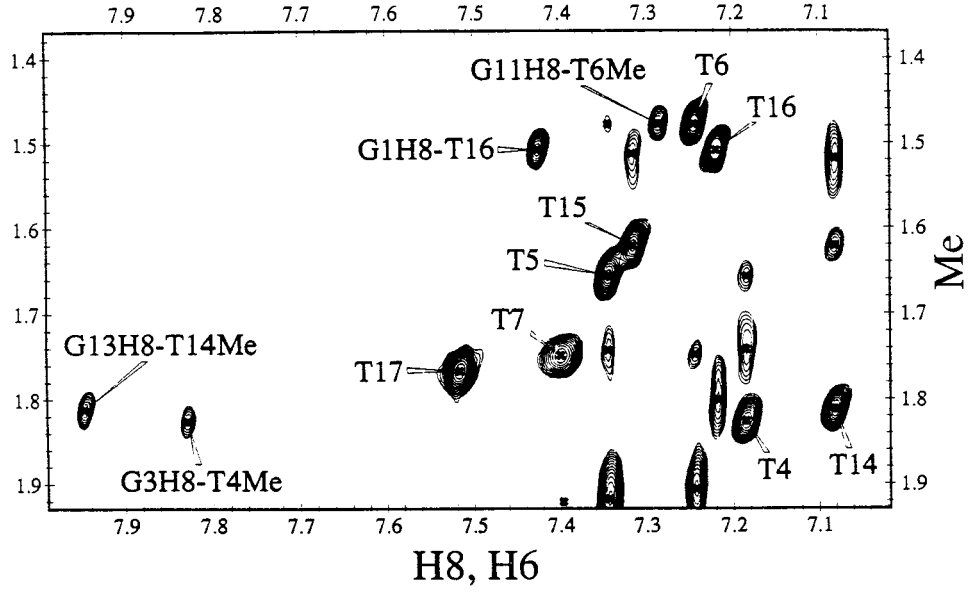

FIGURE 5 The aromatic-methyl proton region of the 150-ms NOESY spectrum of $[d(G_3T_4G_3)]_2$ in 10 mM tk;4Tris (pH 7.5), 30 mM KCl at 20°C. Cross-peaks are observed between T6(methyl)-G11(H8) and T16(methyl)-G1(H8), indicating that these thymine bases stack over the first guanine of the other strand. Also observed is a somewhat greater linewidth for the T7 and T17 intraresidue H6-methyl cross-peaks, suggesting that these residues sample a wider range of local environments.

at 7.51 and 6.12 ppm in figure 2 *B* of our earlier study (Strahan et al., 1994). Significantly, all related intraresidue cross-peaks in the COSY and NOESY spectra are similarly affected. Only thymine protons exhibited these spectral qualities, and the linebroadening of these T7 and T17 protons appears to be temperature dependent, although this was not quantitated. These are all indications of a fast exchange between two or more conformations in the loop.

As noted earlier, the initial in vacuo restrained simulations also pointed toward two major, NMR-detectable conformations of the loop regions, and on this basis, representative structures were chosen for the solvated MD simulations with PME. These loops adjust to the presence of water and coordinated cations in a number of ways. By closely following previously published methods (Cheatham and Kollman, 1997), we were able to discern the probability of water oxygen atoms as a function of time around these different loop structures. Fig. 2 provides stereo images of the two loop conformations with their associated water density probabilities. (The discussion that follows applies to both loops in the molecule, even though only one loop may be explicitly mentioned.)

Fig. 2 *A* depicts the stacked loop conformation of the T14–T17 loop in which the T17 base is stacked directly over the outermost quartet. This conformation has several stabilizing factors: hydrogen bonding is suggested between T14 and T17, and a hydrophobic pocket is formed by the methyl groups of T16 and T17, which point toward each other, and is sandwiched between the T15 sugar and the quartet. It is unclear whether the hydrogen bond is an independent, stabilizing factor, or a consequence of the condensation of the bases around K^+, which is also a stabilizing influence. Throughout the time course of these simulations, the tight contraction of thymines around the K^+ prevented water from entering the interiors of the stacked loops, unless a loop changed its conformation (see below). Instead, the water molecules have their greatest probability just outside of the loops, where the O4 of T14, T15, and T17 are all in close proximity, suggesting a water-mediated hydrogen bonding network external to the loop.

The K^+ structures in unstacked conformations do not have similar hydrophobic pockets, but have water-mediated interactions with the nearest caged K^+ cation. Fig. 2 *B* displays an "unstacked" loop conformation in which T17 is tilted such that its methyl group is stacked above the T15 aromatic base, and most of T17 is exposed to the solvent, where it accesses a wide range of positional variants. The unstacked conformation also has an open central site within the loop, allowing water molecules to enter as they attempt to hydrate the cation. A range of one to three water molecules is observed to occupy this cavity, preferring the position directly above the K^+.

Even though each of the starting structures for each of the three trajectories was well equilibrated with the NMR restraints via in vacuo MD simulations, one of the loops in simulation "rA" underwent a significant conformational change ~100 ps into the restrained PME-MD simulation in water: the T4–T7 loop converted from a "quartet-stacked" conformation (as in Fig. 2 *A*) to an "unstacked" conformation (as in Fig. 2 *B*).

This conformational change occurred with negligible alterations in the NMR restraint violations. As depicted in Fig. 6, the violations of some restraints are counterbalanced by improvements in others: this change causes the NMR restraint distance for T6(H6)–T7(C5) to switch from being stable at ~4 Å to being stable at ~6 Å (Fig. 6 *B*), whereas the T5(H2″)–T7(C5) restraint distance changes in a nearly exactly opposite manner. This unstacking of T7 allows 1–3 water molecules to enter the interior of the loop, where they are stabilized by hydrogen bonding to T5 and electrostatic attractions with the caged K^+. These water molecules inhibit reversion to the stacked conformation during the studied time scales, but T7 continues to sample a range of positions (Fig. 6 *A*).

How well do these two loop conformations satisfy the NMR restraints? Are they equally probable in solution? The

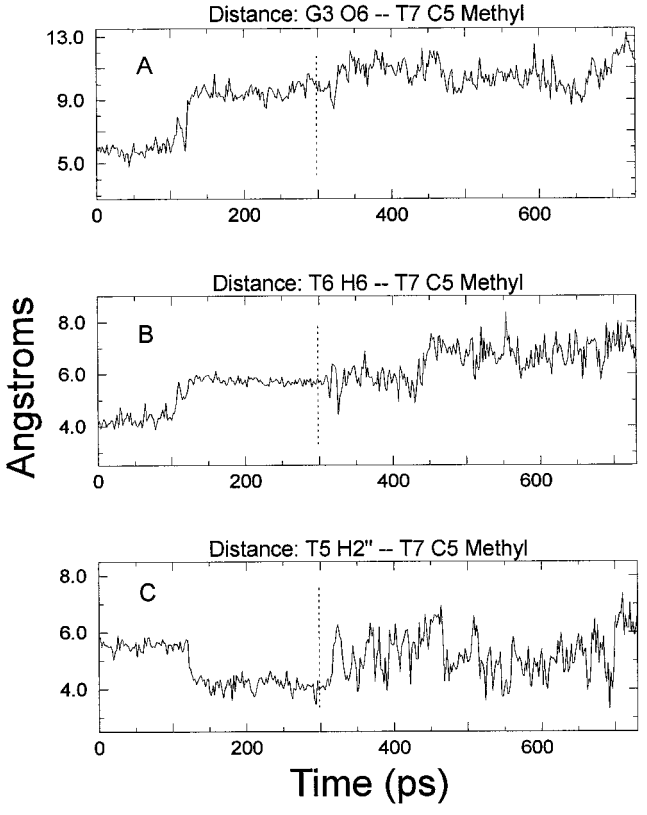

FIGURE 6 Time-dependent distances demonstrating how the T4–T7 loop in trajectory *A* transforms from "quartet stacked" to "unstacked" while satisfying the NMR restraints nearly equally well in both conformations. (*A*) At ~100 ps, T7 moves away from the outermost quartet, as measured by the distance between the C5 methyl and G3(O6), which resides close to the center of the quartet. (*B*) An NMR NOESY cross-peak of medium-weak intensity is seen between T6H6 and T7 methyl; initially this restraint is satisfied, but it is violated after the conformational change. (*C*) A medium-weak intensity NMR NOESY cross-peak was observed between T5(H2″) and T7(methyl); initially this restraint is violated, but it is usually satisfied after the conformational change. The vertical line at 300 ps indicates the point at which restraint force constants were set at zero.

calculation of both standard and sixth-root *R*-factors for an ensemble of structures is one way to determine how well a set of structures fit the NMR data. The structures from the last 100 ps of trajectories rA1, rA2, rB, rC, uA2, uB, and uC were individually analyzed via the CORMA program to determine the *R*-factors for each trajectory. Then all of the structures from trajectories rA, rB, and rC were combined and analyzed as group 1, and those from uA, uB, and uC were combined and analyzed as group 2. Instead of calculating overall, cross-ensemble *R*-factors for these two groups, the PARSE algorithm (Ulyanov et al., 1995) was used.

PARSE analysis selected 11 structures from the rMD-PME trajectories (group 1); within this set, there is a calculated probability of 77% that any given loop will be in an unstacked conformation, and a 23% probability that it will be in a stacked conformation. Of those loops in the stacked conformation, however, 19% will involve the T4–T7 loop, and 81% will involve the T14–T17 loop. Similarly, 12 structures were chosen from the unrestrained PME-MD simulations (group 2), with 76% of the loops calculated to occur in unstacked conformations and 24% in stacked conformations. Because trajectory A converted its loop conformation, there were no unrestrained structures with the T7 residue stacked over the quartet. However, 49% of the T14–T17 loops are calculated to be in the stacked conformation. These percentages are sensitive to a great many parameters, but they clearly establish that stacked and unstacked conformations coexist in significant numbers.

The distribution of loops in the stacked conformation can also be inferred directly from the NMR data. At 2°C, a set of guanine imino protons was observed to have NOE contacts with both the H6 and methyl protons of T7, as well as with its sugar protons. A similar set of contacts was also observed to involve the protons of T17. Because these imino protons participate in the hydrogen bonding within the outermost G-quartets, these observations amount to the direct observation of "quartet-stacked" T7 and T17 bases. The T7 imino proton NOE cross-peaks were nearly identical in intensity to those of the corresponding T17 imino proton cross-peaks (data not shown), indicating that the population of molecules with T7 stacked over the guanine quartet should be nearly equal to the population with T17 stacked. This result differs quantitatively from that of the PARSE analysis above, probably because of the conversion of the T4–T7 loop from stacked to unstacked, hence reducing the sampling of structures with this characteristic.

We conclude that the unstacked population is likely to be slightly larger than the stacked population, and that the two loops have approximately the same probabilities of exploring the two conformations. On the time scales that we have investigated, the presence of water seems to prevent conversion from unstacked to stacked, but may help conversion from stacked to unstacked. However, in the absence of restraints, all solvated conformations are stable for at least 0.5 ns without any significant conformational changes (data not shown).

Comparison of K^+ and Na^+ loop structures

Both of the loop conformations found in these studies with K^+ are different from the compact loop conformation previously determined for the Na^+-stabilized structure (Keniry et al., 1995). The NMR restraint data indicate that these two molecules differ in the details of their hydrophobic and hydrogen bonding interactions. However, the most singularly important difference between them, based solely upon the NMR data, is the existence of multiple loop conformations in the K^+ stabilized structure, but not in the Na^+ structure (Keniry et al., 1995).

One rationale for this and the other differences is based upon the size of the cation; as noted by others (Ross and Hardin, 1994), the smaller size and greater charge density of the Na^+ ion may cause greater contraction of the DNA bases around the cation, limited by steric and geometric requirements. This suggests that with the smaller radius of the sodium ion (Na^+: $r^* = 1.39$ Å versus K^+: $r^* = 1.93$ Å; Ross and Hardin, 1994), the system may try to shrink to optimize coordination with sodium cations and thereby eliminate one of the possible loop conformations. The Na^+ quadruplex, being restricted in its range of motion, has insufficient room for the T7 (or T17) thymine to form transient hydrogen bonds with T4 (T14); nor can it form a hydrophobic pocket between T6 and T5. Instead, the Na^+ T6 forms a hydrogen bond with T4. Hence the multiple conformations in the K^+ form may be due to the comparatively larger ionic radius of the cation, which exerts fewer positional constraints on the thymines in the loop.

Comparative stability of the K^+ and Na^+ hairpin quadruplexes

Our NMR results do not provide a quantitative measure of the effect of different monovalent cations on the thermodynamic stability of the two hairpin quadruplex structures. However, some significant qualitative differences between the K^+ and Na^+ stabilized forms were observed. As noted above, several days after the addition of KCl to a solution of $d(G_3T_4G_3)$, broad lines began to appear in the NMR spectra. Circular dichroism studies (data not shown) suggested that this new species was the linear, four-stranded quadruplex, which can efficiently stack end to end, giving rise to broad NMR peaks. In contrast, no signs of linear quadruplex species have been observed in the presence of NaCl. Similar observations of related oligonucleotide sequences have been reported by others (Balagurumoorthy et al., 1992).

These results can be explained in terms of kinetic or equilibrium differences. As the linear quadruplex form has not been observed in NaCl after extended incubation times, differences in the equilibrium properties are most likely involved. That is, in the presence of NaCl, the free energy difference, $\Delta\Delta G°$, between the hairpin dimer and linear, four-stranded quadruplex forms is sufficiently large that the equilibrium is dominated by the former, leading to solutions in which only the hairpin dimer species occurs in detectable

concentrations. In the presence of KCl, however, $\Delta\Delta G°$ is significantly smaller, such that detectable amounts of each are observed at equilibrium. The kinetics of forming the four-stranded quadruplex are much slower than for the hairpin dimer structure; hence the latter forms initially in KCl, while several days at NMR concentration are required to develop the former, and thus establish true equilibrium conditions.

These differences in $\Delta\Delta G°$ between quadruplexes in K^+- versus Na^+-containing solutions may arise from differential effects of these cations on either the hairpin or the linear quadruplex forms, or both. Our present studies provide one explanation in terms of differential cation effects on the hairpin dimer species. As pointed out earlier, the larger size of the quartets stabilized by K^+ provides greater loop flexibility, resulting in a weakening of the loop-stabilizing interactions. This may lead to a lower overall stability of the hairpin dimer form in the case of K^+ and, correspondingly, a smaller $\Delta\Delta G°$ between hairpin dimer and linear quadruplexes in KCl compared to NaCl. In accord with this hypothesis, separate experiments carried out in NaCl solution in which the loop constituents of $d(G_3T_4G_3)$ were modified (substituting C for T) revealed that the relative amounts of hairpin dimer and linear quadruplex species formed are highly dependent on the loop sequence (Keniry et al., 1997).

Although differences in cation hydration may affect the relative stabilities of the Na^+ and K^+ forms of the hairpin dimer $[d(G_3T_4G_3)]_2$ quadruplexes, as proposed recently (Hud et al., 1996), it is unlikely that they can explain the observation that only hairpin dimer quadruplexes are formed in Na^+, whereas both hairpin and linear structures are formed in K^+. Furthermore, because signals from a linear, four-stranded quadruplex structure were not observed in the titrations of Hud et al. (1996), those experiments involved a kinetically blocked system rather than true equilibrium populations.

CONCLUSIONS

We have evaluated the dynamics and high-resolution structural features of the $[d(G_3T_4G_3)]_2$ quadruplex in K^+ solution, characterized its major differences with the previously determined Na^+-stabilized structure (Keniry et al., 1995), determined the probable regions of hydration (i.e., the grooves and the interiors of the loops), and assessed factors contributing to the stabilization of linear versus folded quadruplex structures. NMR data were incorporated into the refinement of the K^+ stabilized structure via molecular dynamics simulations in which explicit water molecules and coordinated cations were included, and the long-range electrostatic interactions were treated by the particle mesh Ewald summation method.

The use of solvated PME-MD for NMR structural refinement proved to be a great asset, because a detailed analysis was desired for a system in which both cations and solvent play important stabilizing roles. These simulations produced reliable structures that are superior to those from restrained in vacuo simulations, as they account more accurately for conformational flexibility, reduce structural anomalies, and provide insights into the effects of water and cation on the structures by defining better molecular structure in regions that are hydrophilic. In addition, the *R*-factors reveal that the NMR restraints are also somewhat better satisfied by the solvated PME-MD, over the in vacuo simulations.

Although the extent of cation occupation is still unanswered, the present studies clearly indicate the importance of their inclusion when these species are modeled. The fact that K^+ and Na^+ stabilize different structural preferences (linear versus folded quadruplexes) may be partly due to the more stable and tightly structured loop found in the presence of Na^+, compared to the flexible loops found in the presence of K^+, these latter being correlated with the larger quartet diameter and cation size of K^+.

The authors gratefully acknowledge many valuable discussions with Thomas Cheatham III, Wilson S. Ross, Nicolai Ulyanov, Jennifer L. Miller, He Liu, Prof. Charles C. Hardin, and Prof. Peter A. Kollman.

This work was supported by grant GM 51650 awarded by the National Institute of General Medical Sciences, National Institutes of Health, Department of Health and Human Services. We also acknowledge the Computer Graphics Laboratory at the University of California–San Francisco for the use of their facilities, supported by grant RR01081 from the Division of Research Resources, National Institutes of Health.

REFERENCES

Balagurumoorthy, P., S. K. Brahmachari, D. Mohanty, M. Bansal, and V. Sasisekharan. 1992. Hairpin and parallel quartet structures for telomeric sequences. *Nucleic Acids Res.* 20:4061–4067.

Berendsen, H. J. C., J. P. M. Postma, W. F. van Gusteren, A. Di Nola, and J. R. Haak. 1984. Molecular dynamics with coupling to an external bath. *J. Chem. Phys.* 81:3684–3690.

Bock, L. C., L. C. Griffin, J. A. Latham, E. H. Vermaas, and J. J. Toole. 1992. Selection of single-stranded DNA molecules that bind and inhibit human thrombin. *Nature.* 355:564–566.

Borgias, B. A., M. Gochin, D. J. Kerwood, and T. L. James. 1990. Relaxation matrix analysis of 2D-NMR data. *Prog. Nucl. Magn. Res. Spectrosc.* 22:83–100.

Borgias, B. A., and T. L. James. 1990. MARDIGRAS—a procedure for matrix analysis of relaxation for discerning geometry of an aqueous structure. *J. Magn. Res.* 87:475–487.

Brahms, S., V. Fritsch, J. G. Brahms, and E. Westhof. 1992. Investigations on the dynamic structures of adenine- and thymine-containing DNA. *J. Mol. Biol.* 223:455–476.

Cheatham, T. E., and P. A. Kollman. 1997. Molecular dynamics simulations highlight the structural differences among DNA:DNA, RNA:RNA, and DNA:RNA hybrid duplexes. *J. Am. Chem. Soc.* 119:4805–4825.

Cheatham, T. E., J. L. Miller, T. Fox, T. A. Darden, and P. A. Kollman. 1995. Molecular dynamics simulations on solvated biomolecular systems—the particle mesh Ewald method leads to stable trajectories of DNA, RNA, and proteins. *J. Am. Chem. Soc.* 117:4193–4194.

Cherepanov, P., J. A. Este, R. F. Rando, J. O. Ojwang, G. Reekmans, R. Steinfeld, G. David, E. De Clercq, and Z. Debyser. 1997. Mode of interaction of G-quartets with the integrase of human immunodeficiency virus type 1. *Mol. Pharmacol.* 52:771–780.

Cornell, W. D., P. Cieplak, C. I. Bayly, I. R. Gould, K. M. Merz, D. M. Ferguson, D. C. Spellmeyer, T. Fox, J. W. Caldwell, and P. A. Kollman. 1995. A second generation force field for the simulation of proteins,

nucleic acids, and organic molecules. *J. Am. Chem. Soc.* 117: 5179–5197.

Davis, D., and A. Bax. 1985. Assignment of complex ^{1}H NMR spectra via two-dimensional homonuclear Hartmann-Hahn spectroscopy. *J. Am. Chem. Soc.* 107:2820–2821.

Deng, H., and W. H. Braunlin. 1996. Kinetics of sodium ion binding to DNA quadruplexes. *J. Mol. Biol.* 255:476–483.

Essmann, U., L. Perera, M. L. Berkowitz, T. Darden, H. Lee, and L. G. Pedersen. 1995. A smooth particle mesh Ewald method. *J. Chem. Phys.* 103:8577–8593.

Ewald, P. 1921. Investigations of crystals by means of Roentgen rays. *Ann. Phys. (Leipzig).* 64:253–264.

Ferrin, T. E., C. C. Huang, and L. E. Javis. 1988. The Midas display system. *J. Mol. Graph.* 6:13–27.

Freeman, R., S. P. Kempsell, and M. H. Levitt. 1980. Radiofrequency pulse sequences which compensate their own imperfections. *J. Magn. Res.* 38:453.

Guschlbauer, W., J. F. Chantot, and D. Thiele. 1990. 4-Stranded nucleic acid structures 25 years later—from guanosine gels to telomere DNA. *J. Biomol. Struct. Dyn.* 8:491–511.

Haasnoot, C. A. G., M. J. J. Blommers, and C. W. Hilbers. 1987. Conformational aspects of hairpin loops in DNA oligonucleotides. *Springer Ser. Biophys.* 1:212–216.

Haasnoot, C. A., C. W. Hilbers, G. A. van der Marel, J. H. van Boom, U. C. Singh, N. Pattabiraman, and P. A. Kollman. 1986. On loop folding in nucleic acid hairpin-type structures. *J. Biomol. Struct. Dyn.* 3:843–857.

Hardin, C. C., M. J. Corregan, D. V. Lieberman, and B. A. Brown. 1997. Allosteric interactions between DNA strands and monovalent cations in DNA quadruplex assembly: thermodynamic evidence for three linked association pathways. *Biochemistry.* 36:15428–15450.

Hardin, C. C., E. Henderson, T. Watson, and J. K. Prosser. 1991. Monovalent cation induced structural transitions in telomeric DNAs: G-DNA folding intermediates. *Biochemistry.* 30:4460–4472.

Hardin, C. C., T. Watson, M. Corregan, and C. Bailey. 1992. Cation-dependent transition between the quadruplex and Watson-Crick hairpin forms of d(CGCG$_3$GCG). *Biochemistry.* 31:833–841.

Harvey, S. C., R. K.-Z. Tan, and T. E. Cheatham. 1998. The flying ice cube: velocity rescaling in molecular dynamics leads to violation of energy equipartition. *J. Comp. Chem.* 19:726–740.

Hore, P. J. 1983. Solvent suppression in Fourier transform nuclear magnetic resonance. *J. Magn. Res.* 55:283–300.

Hud, N. V., F. W. Smith, F. A. Anet, and J. Feigon. 1996. The selectivity for K^+ versus Na^+ in DNA quadruplexes is dominated by relative free energies of hydration: a thermodynamic analysis by ^{1}H NMR. *Biochemistry.* 35:15383–15390.

Kang, C., X. Zhang, R. Ratliff, R. Moyzis, and A. Rich. 1992. Crystal structure of four-stranded *Oxytricha* telomeric DNA. *Nature.* 356: 126–131.

Keniry, M. A., E. A. Owen, and R. H. Shafer. 1997. The contribution of thymine-thymine interactions to the stability of folded dimeric quadruplexes. *Nucleic Acids Res.* 25:4389–4392.

Keniry, M. A., G. D. Strahan, E. A. Owen, and R. H. Shafer. 1995. Solution structure of the Na^+ form of the dimeric guanine quadruplex $[d(G_3T_4G_3)]_2$. *Eur. J. Biochem.* 233:631–643.

Kim, S. G., L. J. Lin, and B. R. Reid. 1992. Determination of nucleic acid backbone conformation by ^{1}H NMR. *Biochemistry.* 31:3564–3574.

Kneller, D. G. 1992. UCSF Sparky: A Graphical NMR Assignment Application. The Sparky User's Manual. University of California, San Francisco.

Laughlan, G., A. I. Murchie, D. G. Norman, M. H. Moore, P. C. Moody, D. M. Lilley, and B. Luisi. 1994. The high-resolution crystal structure of a parallel-stranded guanine tetraplex. *Science.* 265:520–524.

Liu, H., P. D. Thomas, and T. L. James. 1992. Averaging of cross-relaxation rates and distances for methyl, methylene, and aromatic ring protons due to motion or overlap—extraction of accurate distances iteratively via relaxation matrix analysis of 2D-NOE spectra. *J. Magn. Reson.* 98:163–175.

Marion, D., and K. Wuthrich. 1983. Application of phase sensitive two-dimensional correlated spectroscopy (COSY) for measurements of ^{1}H-^{1}H spin-spin coupling constants in proteins. *Biochem. Biophys. Res. Commun.* 113:967–974.

Mazumder, A., N. Neamati, J. O. Ojwang, S. Sunder, R. F. Rando, and Y. Pommier. 1996. Inhibition of the human immunodeficiency virus type 1 integrase by guanosine quartet structures. *Biochemistry.* 35: 13762–13771.

Padmanabhan, K., K. P. Padmanabhan, J. D. Ferrara, J. E. Sadler, and A. Tulinsky. 1993. The structure of alpha-thrombin inhibited by a 15-mer single-stranded DNA aptamer. *J. Biol. Chem.* 268:17651–17654.

Padmanabhan, K., and A. Tulinsky. 1996. An ambiguous structure of a DNA 15-mer thrombin complex. *Acta Crystallogr. D.* 52:272–282.

Pearlman, D., D. A. Case, J. W. Caldwell, W. S. Ross, T. E. Cheatham, D. M. Ferguson, G. L. Seibel, U. C. Singh, P. K. Weiner, and P. A. Kollman. 1995. AMBER 4.1. University of California, San Francisco.

Phillips, K., Z. Dauter, A. I. H. Murchie, D. M. J. Lilley, and B. Luisi. 1997. The crystal structure of a parallel-stranded guanine tetraplex at 0.95 angstrom resolution. *J. Mol. Biol.* 273:171–182.

Ross, W. S., and C. C. Hardin. 1994. Ion-induced stabilization of the G-DNA quadruplex—free energy perturbation studies. *J. Am. Chem. Soc.* 116:6070–6080.

Ryckaert, J. P., G. Cicotti, and H. J. C. Berendsen. 1977. Numerical integration of the Cartesian equations of motion of a system with constraints: molecular dynamics of *n*-alkanes. *J. Comp. Phys.* 23: 327–341.

Scaria, P. V., S. J. Shire, and R. H. Shafer. 1992. Quadruplex structure of d($G_3T_4G_3$) stabilized by K^+ or Na^+ is an asymmetric hairpin dimer. *Proc. Natl. Acad. Sci. USA.* 89:10336–10340.

Schmitz, U., and T. L. James. 1995. How to generate accurate solution structures of double-helical nucleic acid fragments using nuclear magnetic resonance and restrained molecular dynamics. *Methods Enzymol.* 261:3–44.

Schultze, P., F. W. Smith, and J. Feigon. 1994. Refined solution structure of the dimeric quadruplex formed from the *Oxytricha* telomeric oligonucleotide d(GGGGTTTTGGGG). *Structure.* 2:221–233.

Smith, F. W., F. W. Lau, and J. Feigon. 1994. d($G_3T_4G_3$) forms an asymmetric diagonally looped dimeric quadruplex with guanosine 5′-syn-syn-anti and 5′-syn-anti-anti N-glycosidic conformations. *Proc. Natl. Acad. Sci. USA.* 91:10546–10550.

States, D. J., R. A. Haberkorn, and D. J. Ruben. 1982. A two-dimentional nuclear Overhauser experiment with pure absorption phase in four quadrants. *J. Magn. Reson.* 48:286–292.

Strahan, G. D., R. H. Shafer, and M. A. Keniry. 1994. Structural properties of the $[d(G_3T_4G_3)]_2$ quadruplex: evidence for sequential syn-syn deoxyguanosines. *Nucleic Acids Res.* 22:5447–5455.

Sundquist, W. I., and A. Klug. 1989. Telomeric DNA dimerizes by formation of guanine tetrads between hairpin loops. *Nature.* 342: 825–829.

Ulyanov, N. B., U. Schmitz, A. Kumar, and T. L. James. 1995. Probability assessment of conformational ensembles: sugar repuckering in a DNA duplex in solution. *Biophys. J.* 68:13–24.

Williamson, J. R. 1994. G-quartet structures in telomeric DNA. *Annu. Rev. Biophys. Biomol. Struct.* 23:703–730.